Morphology of Micelles Formed by Diblock Copolymer with a Polyelectrolyte Block

O. V. Borisov*,†,‡ and E. B. Zhulina†

Institute of Macromolecular Compounds of the Russian Academy of Sciences, 199004, St. Petersburg, Russia, and Max Planck Institut für Polymerforschung, Ackermann weg 2, 55128, Mainz, Germany

Received September 3, 2003; Revised Manuscript Received October 20, 2003

ABSTRACT: We present a mean-field theory to describe micelles formed by diblock copolymer with one neutral and one polyelectrolyte block in dilute aqueous solution. We examine equilibrium parameters of micelles as a function of degree of polymerization of both blocks, fraction of charged monomers in the ionic block, and the ionic strength in the solution. In contrast to earlier scaling studies, our theory enables us to construct phase diagrams of the system and distinguish the ranges of thermodynamic stability of spherical, cylindrical, and lamellar aggregates. We demonstrate that spherical starlike or crew-cut micelles are thermodynamically stable in a range of moderate salt concentrations. The morphological sphere-to-cylinder and cylinder-to-lamella transitions of the aggregates are predicted to occur for crew-cut micelles upon an increase in salt concentration or/and a decrease in degree of ionization of corona (ionic) block. The driving force for morphological transitions is the gain in conformational entropy of nonionic core block.

1. Introduction

Diblock copolymers with hydrophilic and hydrophobic blocks constitute an important class of polymeric surfactants. Their features include the surface activity and the ability to self-assembly into micellar-like aggregates and mesophases of different morphologies. Coassembly of the copolymers with hydrophobic substances gives rise to micelles with swollen cores. The latter effect (solubilization, encapsulation) determines an outstanding importance of the amphiphilic copolymers for the purposes of controlled encapsulation, delivery and release of drugs, agrochemicals, design of nanoreactors, etc.

The structure and morphology of self-assembled aggregates of diblock copolymers are determined by the lyophilic/lyophobic balance in the copolymer chain. This balance is determined by block copolymer composition (degrees of polymerization of the blocks) and by the strength of attractive and repulsive interactions between monomers in the core and in the corona, respectively.

When the hydrophilic block is charged (and constitutes a polyelectrolyte), the copolymer aggregation behavior is similar to that of the ionic surfactant. The most important features of ionic surfactants[1,2] are determined by the electrostatic interactions between the hydrophilic groups. The strength of the Coulomb repulsion between the ionic groups depends on the ionic strength of the solution (determined by the bulk concentrations of salt and surfactant). An additional "degree of freedom" appears in the case of pH-sensitive ionic groups (that is, when the degree of ionization can be varied by changing the pH in the solution). By tuning the strength of the Coulomb repulsion between the ionic groups, one can affect the structure and morphology of the aggregates. Typically, the transitions from spherical to cylindrical and further to lamellar-like aggregates are observed upon an increase in the ionic strength of the solution due to progressive screening of the electrostatic interactions.

Amphiphilic diblock copolymers with a polyelectrolyte block were extensively studied experimentally during recent years.[3−15] The presence of spherical micelles with a dense hydrophobic core and extended charged corona was detected by static light scattering (SLS) and small-angle neutron scattering (SANS) experiments in dilute solutions of diblock copolymer with a long polyelectrolye block and a short hydrophobic (aliphatic) block. Other morphologies, e.g., cylindrical micelles and vesicles, were detected[11−14] for ionic/nonionic copolymer with relatively long hydrophobic blocks.

Numerous experiments were performed on copolymers with partially sulfonated polystyrene (PS/PSS) block. Because of the large dissociation constant of PSS, all the sulfonated monomers are ionized in water solution irrespective of the ionic strength or pH. In another set of experiments the poly(acrylic)acid was used as a polyelectrolyte block.[9] In contrast to sulfonic acid, acrylic (or methacrylic) acid is a weakly dissociating polyelectrolyte (p$K \approx 4.7$), and the degree of dissociation of acidic monomers depends strongly on the local pH. Most of experiments deal with PAA at sufficiently high pH > pK and large salt concentration. Under these conditions, the degree of ionization of PAA block is close to unity for both associated in micelles and free block copolymer molecules. Remarkably, the situation is qualitatively different in the solution of lower pH ∼ pK, when the strong interference between ionization and association equilibria occurs.

The equilibrium structure of charged spherical micelles in salt-free solutions of diblock copolymers was analyzed in a number of theoretical studies.[16−19] In our recent work,[20] we systematically explored the effect of the ionic strength in the solution on thermodynamics of micellization of the copolymer with a hydrophobic and a strongly dissociating ("quenched") polyelectrolyte block. We demonstrated that an increase in the ionic strength

† Russian Academy of Sciences.
‡ Max Planck Institut für Polymerforschung.

10.1021/ma0304628 CCC: $25.00
Published on Web 11/27/2003

results in the increase in micelle aggregation number and, simultaneously, in a weak decrease in the thickness of micellar corona due to enhancing screening of the Coulomb repulsion between the corona blocks. The analysis in ref 20 enabled us to relate the results for charged micelles in the high salt limit to the quasi-neutral behavior described by the scaling theory of neutral block copolymer micelles.[22−24] The predicted exponents for the power law dependence of micelle size as a function of the salt concentration were confirmed by recent observations of Förster et al.[10]

The aggregation behavior becomes more sophisticated in the case of diblock copolymer with weakly ionizable polyelectrolyte block. As has been demonstrated in ref 21, the interference between ionization and association equilibria is the key point in understanding the self-assembly of block copolymers with a weak polyelectrolyte block. In contrast to aggregates with strong polyelectrolyte block, micelles with weakly ionizable corona can experience abrupt transformations without change in morphology. Namely, the spherical micelles can abruptly decrease the aggregation number and change the shape in response to enhanced corona ionization caused by an increase in the ionic strength of the solution. The origin of this effect is the different local pH inside the weak polyelectrolyte corona as compared to the pH in the bulk solution.

The goal of the present paper is a systematic study of the equilibrium phase diagrams that determine the ranges of thermodynamic stability for charged micelles of different shapes and morphologies. We focus on the conditions of relatively high ionic strength in the solution when the difference between strong and weak polyelectrolytes is negligible, and the polyelectrolyte corona is characterized by the same degree of ionization as a single chain in the bulk solution. We demonstrate that an increase in the ionic strength of the solution leads to the sphere-to-cylinder and cylinder-to-lamella morphological transitions. In contrast to earlier study,[25] we find that these transitions occur when the micelle has the so-called crew-cut shape (that is, when the thickness of corona is noticeably smaller than the core size). We explore the equilibrium parameters of micelles with different morphologies and delineate the scaling laws for the transition lines (binodals) that separate spherical, cylindrical, and lamellar aggregates.

The rest of the paper is organized as follows. In section 2 we present the theoretical model to analyze the structure and morphology of diblock copolymer micelle in dilute aqueous solution. General formalism is presented in section 3. The corona free energies of spherical, cylindrical, and lamellar aggregates are derived in the Appendix. In section 4 we present the phase diagrams of the system and analyze the equilibrium micelle characteristics as a function of salt concentration, degree of corona ionization, and degrees of polymerization of the blocks. The conclusions are summarized in section 5.

2. Model

We consider a dilute aqueous solution of diblock copolymer, each comprising a hydrophobic block (with degree of polymerization N_B) and a polyelectrolyte block (with degree of polymerization N_A).

Both blocks are assumed to be intrinsically flexible. (The statistical segment length is of the order of a monomer unit length a, which is taken as the unit length in our subsequent analysis.) The polyelectrolyte block is weakly charged, i.e., comprises the fraction $\alpha \leq (a/l_B)^2 \cong 1$ of charged monomers. Here $l_B = e^2/k_B T\epsilon$ is the Bjerrum length, which is of order 0.7 nm in water under normal conditions (e is the elementary charge, ϵ is the dielectric constant of the solvent, T is the temperature, and k_B is the Boltzmann constant). The fraction of charged monomers α is either quenched (i.e., depends only on the primary sequence like for partially sulfonated PS) or can be tuned by the variation of the pH in the solution in the cases of pH-sensitive (weakly dissociating, like PAA) polyelectrolyte blocks.[26] The solution contains small mobile counterions which compensate the overall charge αN of each macroion and, in general case, also co-ions and counterions of added salt. All mobile ions are assumed to be monovalent. The salt concentration, c_s, in the bulk of the solution determines the Debye screening length, $\kappa^{-1} = (8\pi l_B c_s)^{-1/2}$.

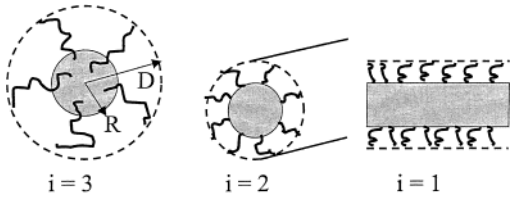

Figure 1. Self-assembled aggregates of block copolymers of spherical, cylindrical, and lamellar morphologies; N_A is the number of monomers in the hydrophilic block, and N_B is the number of monomers in the hydrophobic block. R is the radius of the core, and D is the radius of corona.

The short-range (van der Waals) interactions between monomers are modeled in terms of the virial expansion of the nonelectrostatic free energy. The corresponding dimensionless second, v_A, v_B, and third, w_A, w_B, virial coefficients are normalized by the factors a^{-3} and a^{-6}, respectively. We assume that water is a poor solvent for the hydrophobic block B so that $v_B \cong (\theta_B - T)/\theta_B \cong -\tau \leq 0$, where θ_B is θ-temperature for block B. On the contrary, for monomers of a polyelectrolyte block water is assumed to be a marginal good solvent so that $v_A \geq 0$. We remark that for hydrophobic polyelectrolytes, like poly(styrenesulfonate), binary interactions between noncharged monomers in water are attractive. However, as long as Coulomb repulsion ensures strong extension of the polyelectrolyte chains (that is the case at sufficiently high fraction of charged monomers), this binary short-range attraction does not affect the chain conformation and can be neglected.

The third virial coefficients, w_A, w_B, are virtually independent of T and are of the order of unity. The virial coefficients describing A−B monomer−monomer interactions are not relevant in the strong segregation limit considered here.

When the polymer concentration in solution exceeds the so-called critical micelle concentration (cmc), the block copolymer chains associate to form micelles. A micelle consists of the hydrophobic core comprising collapsed blocks B that is surrounded by the polyelectrolyte corona of blocks A (Figure 1). We assume the strong segregation limit, i.e., $\tau \sim 1$, so that the width of the core/corona boundary is small compared to the size of the micelle. Therefore, blocks A and B are envisioned as grafted to the core/corona interface. The morphology of micelles is specified by index i. We consider here the spherical ($i = 3$), cylindrical ($i = 2$), or lamellar-like ($i = 1$) aggregates.

An important structural and thermodynamic characteristic of a micelle of any morphology is the area s of the core−water interface per copolymer chain. In the case of a spherical micelle area s determines the aggregation number p as $p = 4\pi R^2/s$, whereas in the case of a cylindrical micelle the number of chains per unit length of the cylinder h^{-1} is expressed as $h = s/2\pi R$, where R is the radius of the core.

3. General Formalism

The equilibrium structure and the free energy $F^{(i)}$ per chain in the micelle of morphology i is determined by the balance of the excess free energy of the water−core interface, $F_{\text{interface}}(s)$, and the free energies of the core, $F_{\text{core}}(s)$, and of the corona, $F_{\text{corona}}(s)$. Here, s is the area of the core−water interface per chain and $i = 1$, 2, and 3 for lamella, cylinder, and sphere, respectively. The collapsed core of the micelle is characterized (see e.g. ref 27) by the uniform polymer density τ. This packing constraint imposes the relation between the core radius R and the core interface area s per chain in the aggregate of morphology i as

$$s = s^{(i)}(R) = \frac{iN_B}{\tau R} \quad i = 1, 2, 3 \tag{1}$$

To calculate the free energies of micelles, we generalize the earlier model[23] used to construct the scaling phase diagram for a neutral block copolymer micelle in a selective solvent. The polyelectrolyte nature of the corona is taken into account in a mean-field (local osmotic balance) approximation, which is applicable in a wide range of ionic strengths of the solution (in the salt-dominance regime).[20]

The value of $s = s_{\min}$ corresponding to the minimal free energy per chain in the aggregate of given morphology can be found by minimizing the free energy of the micelle

$$F^{(i)}(s) = F^{(i)}_{\text{corona}}(s) + F^{(i)}_{\text{core}}(s) + F_{\text{interface}}(s) \tag{2}$$

calculated per one chain.

3.1. Free Energies of the Core and of the Interface. The excess free energy of the core−water interface per chain in the aggregate of the morphology i is given by

$$F^{(i)}_{\text{interface}}(R)/k_BT = \gamma s(R) \cong i\gamma N_B/\tau R \quad i = 1, 2, 3 \tag{3}$$

where $k_BT\gamma \cong k_BT\tau^2$ is the surface free energy per unit area at the core−water interface.

The elastic free energy of the extended core blocks per chain yields

$$\frac{F^{(i)}_{\text{core}}(R)}{k_BT} = b_i\frac{R^2}{N_B} \tag{4}$$

where

$$b_i = \begin{cases} \pi^2/8 & i = 1 \\ \pi^2/16 & i = 2 \\ 3\pi^2/80 & i = 3 \end{cases} \tag{5}$$

The latter equation takes into account that the uniform core density constraint imposes nonuniform and nonequal extension of the core blocks.[28]

We note that the free energy of nonelectrostatic interactions in the collapsed core does not depend on the structural parameters of the micelle (it is determined only by the values of $v_B \simeq \tau$, w_B, and N_B), and we omit this contribution from further consideration.

3.2. Free Energy of Corona. Because of the narrow core/corona interface, we consider the charged corona of a micelle as a curved (in a spherical, $i = 3$, or cylindrical, $i = 2$, micelle) or as a planar (in a lamellar aggregate, $i = 1$) polyelectrolyte brush.[29−31] To calculate the free energy of the polyelectrolyte brush, we employ the combination of the mean-field and the local electroneutrality approximations. The latter one assumes that the local excess (number) density of counterions inside the corona is approximately equal to the local (number) density of charged monomers. This condition ensures the local (and the total) electroneutrality of the micellar corona. As demonstrated in refs 29−31 and also confirmed experimentally,[32,33] the local electroneutrality approximation is justified even in a salt-free solution provided that the number of polyelectrolyte chains in the corona is sufficiently large. In other words, because of the strong Coulomb attraction to the polyelectrolyte blocks, most of the counterions are retained inside the micellar corona even in the salt-free regime.

We assume in the subsequent analysis that the condition of salt dominance[34] in the micellar corona is fulfilled in the whole range of the salt concentrations considered. As was demonstrated in ref 20, the mean-field approximation is valid in the salt dominance regime, unless salt concentration becomes too high. However, the quantitative deviation from the mean-field results remains small in the whole salt-dominance regime. Within the mean-field approximation we can describe the structure and thermodynamics of the polyelectrolyte brush similarly to those of a neutral brush in a good solvent (that is, under conditions when the repulsive short-range binary interactions between monomers are dominant). In the case of salt-dominated polyelectrolyte brush this short-range repulsion is governed by the screened (by salt) Coulomb interactions between charged monomers complemented by the nonelectrostatic (excluded volume) interactions. The effective second virial coefficient calculated per monomer is then equal to

$$v = v_A + \alpha^2/4c_s \tag{6}$$

where $v_A \lesssim 1$ is the bare nonelectrostatic contribution to the second virial coefficient. We remark that eq 6 is based on the mean-field approximation applied below and follows from additivity of the short-range and electrostatic interactions. The explicit form of the second term (the electrostatic contribution) can be obtained on the basis of the osmotic balance arguments (see e.g. refs 29 and 36). Upon an increase in salt concentration c_s or/and decrease in the degree of ionization α, $v \to v_A$. Hence, the analysis of the morphology of the micellar aggregates formed by diblock copolymer with polyelectrolyte block is reduced to that of a neutral copolymer with variable solvent strength for the corona block.

The free energy of the corona of aggregates of different morphologies is calculated in the Appendix.

The corona free energy per chain in micelle of morphology i yields

$$F^{(i)}_{\text{corona}}(R)/k_BT = \frac{3^{8/3}}{2(4-i)}\left(\frac{\tau v}{iN_B}\right)^{1/3} R^{4/3}\left[\left(1+\frac{i+2}{3^{4/3}}\left(\frac{\tau v}{iN_B}\right)^{1/3}\frac{N_A}{R^{2/3}}\right)^{(4-i)/(i+2)} - 1\right] \quad (7)$$

whereas the thickness of the corona is given by

$$D(R) = R\left[1+\frac{i+2}{3^{4/3}}\left(\frac{\tau v}{iN_B}\right)^{1/3}\frac{N_A}{R^{2/3}}\right]^{3/(i+2)} \quad (8)$$

In the asymptotic limit $(\tau v/N_B)^{1/3}N_A/R^{2/3} \gg 1$, corresponding to $D \gg R$, eqs 7 and 8 assume the form

$$F^{(i)}_{\text{corona}} \approx \frac{3^{4i/(i+2)}}{2(4-i)}(i+2)^{(4-i)/(i+2)}\left(\frac{\tau v}{iN_B}\right)^{2/(i+2)} R^{2i/(i+2)} N_A{}^{(4-i)/(i+2)} \quad (9)$$

and

$$D \approx \left(\frac{i+2}{3^{4/3}}\right)^{3/(i+2)}\left(\frac{\tau v}{iN_B}\right)^{1/(i+2)} N_A{}^{3/(i+2)} R^{i/(i+2)} \quad (10)$$

In the opposite limit$(\tau v/N_B)^{1/3}N_A/R^{2/3} \ll 1$ corresponding to $D - R \ll R$ (i.e., the corona is envisioned as a quasi-planar brush)

$$F^{(i)}_{\text{corona}} \approx F^{(1)}_{\text{corona}}\left(1+\frac{(1-i)}{3}\frac{H^{(1)}}{R}\right) \quad (11)$$

and

$$D - R \approx H^{(1)}\left(1+\frac{(1-i)}{6}\frac{H^{(1)}}{R}\right) \quad (12)$$

Here

$$F^{(1)}_{\text{corona}} = \frac{3^{4/3}}{2}N_A v^{2/3} s^{-2/3} \quad (13)$$

and

$$H^{(1)} = \frac{1}{3^{1/3}}N_A v^{1/3} s^{-1/3} \quad (14)$$

are the corona contribution to the free energy and the corona thickness in the lamellar structure with the area s per chain.

3.3. Phase Diagram. Equations 2, 4, 3, and 7 determine the free energy per chain in an aggregate of morphology $i = 1, 2, 3$ as a function of the core radius R. Minimization of $F^{(i)}$ with respect to R gives the equilibrium core radius $R = R^{(i)}_{\text{min}}$ in aggregate of morphology $i = 1, 2, 3$ at given external conditions. By using eqs 2, 4, 3, and 7, one can calculate the free energy, $F^{(i)}$, per chain in the aggregate of morphology $i = 1, 2, 3$. Equation 8 provides the corona thickness $H^{(i)} = D^{(i)} - R^{(i)}$ for given values of N_A, N_B, τ, and v. The effective second virial coefficient v is determined by salt concentration and degree of ionization of the polyelectrolyte block according to eq 6.

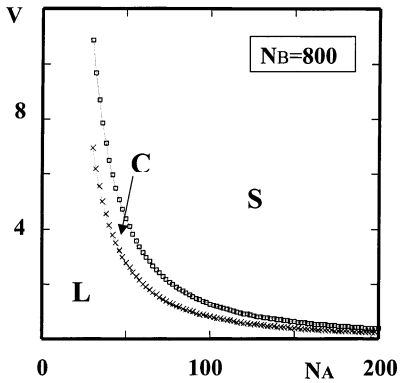

Figure 2. Diagram of states for diblock copolymer aggregates in (v, N_A) coordinates. Values of v corresponding to sphere-to-cylinder and cylinder-to-lamella transitions (boundaries between different regions) are indicated by boxes and crosses, respectively.

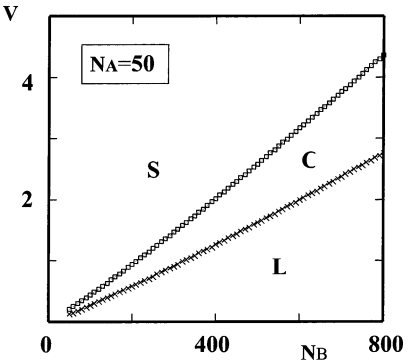

Figure 3. Diagram of states in (v, N_B) coordinates. Regions of thermodynamic stability of spherical (S), cylindrical (C), and lamellar (L) aggregates are indicated.

The free energy $F^{(i)} \equiv F^{(i)}(R_{\text{min}})$ is the equilibrium free energy per chain in the aggregate of given morphology i. At given values of N_A, N_B, τ, and v, the morphology which has the lowest free energy, $F = \min\{F^{(i)}\}$, is thermodynamically stable. The transition between morphologies i and $i \pm 1$ occurs when $F^{(i)} = F^{(i\pm1)}$. This condition determines the binodal line between the neighboring morphologies.

The critical micelle concentration, cmc (that is, the concentration of unimers in the solution that are in equilibrium with copolymer molecules in the aggregate), can be found as

$$\ln \text{cmc} \approx (F - F_0)/k_BT \quad (15)$$

where F_0 is the free energy (standard chemical potential) of a single copolymer chain (unimer) in the solution.

4. Results

Typical phase diagrams of the system in the v, N_A and v, N_B coordinates are presented in Figure 2 and Figure 3, respectively. Both diagrams contain the regions corresponding to spherical (S), cylindrical (C), and lamellar-like (L) aggregates. A progressive decrease in the effective second virial coefficient $v \simeq \alpha^2/c_s$ due to an increase in salt concentration c_s leads to successive sphere-to-cylinder and cylinder-to-lamella transitions. Spherical aggregates are stable in a wide range of the effective second virial coefficient v (or, equivalently, of salt concentration c_s) if $N_A/N_B \geq 1$ and even for asymmetric, $N_A/N_B \leq 1$, copolymer. The ranges of stability

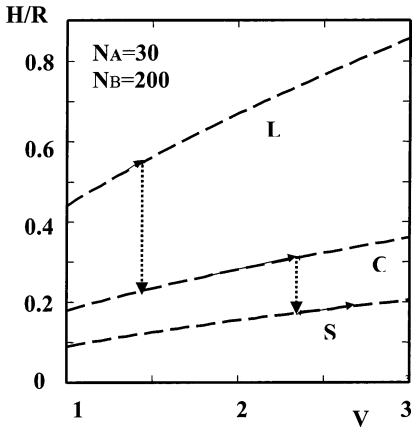

Figure 4. Ratio of corona thickness $H = D - R$ to core radius R as a function of the effective virial coefficient v in aggregates of lamellar (L), cylindrical (C), and spherical (S) morphologies. Arrows indicate the lamellar-to-cylinder and cylinder-to-sphere transitions.

of the cylindrical and lamellar aggregates increase with increasing $N_B \gg N_A$.

Within each morphology, a decrease in $v = \alpha^2/c_s$ leads to the increase in core radius R and the weak decrease in corona thickness $D - R$. Slight shrinking of the corona is the result of two opposite trends: increasing crowding of the corona chains and decreasing strength of the Coulomb repulsion between them. Therefore, the ratio $(D - R)/R$ increases as a function of v (see Figure 4). At the binodal lines in Figures 2 and 3, corresponding to the sphere-to-cylinder (S → C) and cylinder-to-lamella (C → L) transitions, the core radius R drops abruptly leading to elastic relaxation of the core blocks, whereas extension of the corona chains jumps up. As a result, the ratio H/R also jumps up in the transition point and then continues to decrease upon further decrease in v. As we demonstrate below, it is relaxation in elastic stretching of the core blocks that causes the sphere-to-cylinder and cylinder-to-lamella morphological transitions.

To address this issue in more detail, we consider two asymptotic limits, $D \gg R$ (corresponding to the so-called starlike micelles) and $D - R \ll R$ (corresponding to the so-called "crew-cut" micelles).

4.1. Starlike Micelles. Structural characteristics of micelles in the starlike regime can be obtained by balancing the interfacial free energy $F_{interface}$ given by eq 3 and the asymptotic form of the corona free energy given by eq 9. The contribution of the core blocks, F_{core}, in this regime is negligible. In particular, the free energy of the star like micelle is given by

$$F^{(i)} \approx \frac{1}{2}\left(\frac{9}{i}\right)^{2i/(3i+2)}(3i+2)\frac{3i+2}{(4-i)^{(i+2)/(3i+2)}} \times (i+2)^{2(1-i)/(3i+2)}\left(\frac{iN_B}{\tau v}\right)^{2(i-1)/(3i+2)}\gamma^{2i/(3i+2)}v^{2/(3i+2)}N_A^{(4-i)/(3i+2)} \quad (16)$$

while the size of the micellar corona is given by

$$D \approx \left(\frac{4-i}{i}\right)^{i/(3i+2)}(i+2)^{(2i+3)/(3i+2)}3^{-4(i+1)/(3i+2)} \times \left(\frac{iN_B}{\tau v}\right)^{(i-1)/(3i+2)}\gamma^{i/(3i+2)}v^{1/(3i+2)}N_A^{(i+3)/(3i+2)} \quad (17)$$

One can easily check that, for starlike micelles of all the morphologies with $D^{(i)} \gg R^{(i)}$ $(i = 1, 2, 3)$, $F^{(3)} \ll F^{(2)} \ll F^{(1)}$ as long as $v \gg (N_B/\tau)^{5/3}N_A^{-7/3}\gamma^{2/3}$. Hence, for aggregates with large corona, $D \gg R$, the spherical starlike micelles are thermodynamically favorable. This is due to the geometry of the corona, minimizing the overlap and the repulsive interaction between the coronal blocks. Here, the contribution due to extension of the core blocks is negligible.

4.2. Crew-Cut Micelles. Structural and thermodynamic properties of the crew-cut, $D - R \ll R$, micelles can be obtained by using eq 11 for the corona free energy. As is seen from eq 11, for crew-cut micelles the dominant contribution to the corona free energy is the same for aggregates of all the considered morphologies, whereas the correction terms appearing for $i = 2$ and 3 account for the difference between spherical and cylindrical morphologies. (In a spherical corona the chains are less crowded and experience weaker repulsion than in a cylindrical corona.)

As follows from minimization of the free energy (see also Figure 4), the morphological transitions occur in the range of conditions where $D - R \ll R$, that is, when the micelles have the crew-cut shape. Therefore, we can use the expansion of the free energy of the corona, eq 11, to derive approximate analytical expressions for the binodal lines as a function of molecular weights of blocks, N_A and N_B, and degree of corona ionization α. For crew-cut micelles, the free energy acquires the following form

$$F^{(i)} \approx F^{(1)}(s) - \frac{i-1}{2i}\frac{N_A^2 v\tau}{N_B} + \frac{i\gamma N_B}{\tau R} + b_i\frac{R^2}{N_B} \qquad i = 1, 2, 3 \quad (18)$$

where $s = s^{(i)}(R)$ as given by eq 1. Here, the first term is the free energy of planar corona. The second (negative) term is the correction due to the cylindrical or spherical shape of the micelle. In framework of the mean-field approximation, it does not depend on core radius R but varies with micelle morphology. (For spherical micelle, $i = 3$, a decrease in the corona free energy due to the curvature is larger than for cylindrical micelle, $i = 2$.) The third term is the surface free energy of corona/core interface, whereas the last term describes the elastic stretching of the core blocks. We note that in the crew-cut regime the core contribution (the last term on the right-hand side in eq 18) is still small with respect to the first (the main) term in the corona free energy. Therefore, the equilibrium radius of the micelle is determined predominantly by the balance of the first and the third terms in eq 18, whereas the forth term induces only small correction.

Minimization of the free energy, eq 18, gives with the accuracy of quadratic terms

$$F^{(i)} \approx \frac{5}{2}3^{1/5}N_A^{3/5}v^{2/5}\gamma^{2/5} - \frac{i-1}{2i}\frac{N_A^2 v\tau}{N_B} + b_i\frac{i^2}{3^{2/5}}\frac{N_B}{\tau^2} \times \left(\frac{\gamma}{N_A v^{2/5}}\right)^{6/5} \qquad i = 1, 2, 3 \quad (19)$$

The approximate expression for binodal line corresponding to the transition from morphology $i + 1$ to i

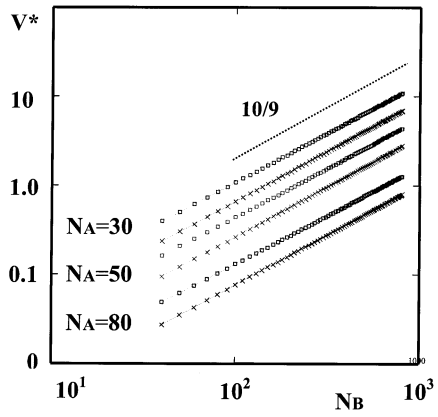

Figure 5. Values of the effective virial coefficient, v^*, corresponding to sphere-to-cylinder (boxes) and cylinder-to-lamella (crosses) transitions as a function of the number of monomers in the core block, N_B. Values of N_A corresponding to different curves are indicated. The slope 10/9 is shown by the dotted line.

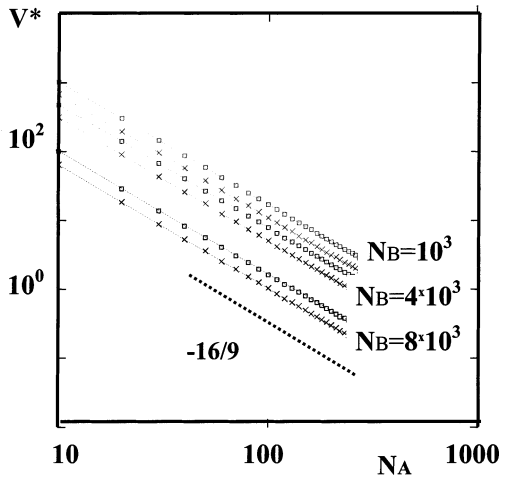

Figure 6. Values of the effective virial coefficient, v^*, corresponding to sphere-to-cylinder (boxes) and cylinder-to-lamella (crosses) transitions as a function of the number of monomers in the corona block, N_A. Values of N_B corresponding to different curves are indicated. The slope −16/9 is shown by the dotted line.

($i = 2, 1$) is then given by

$$v \approx \frac{N_B^{10/9}}{N_A^{16/9}} \frac{\gamma^{2/3}}{\tau^{5/3}} \left[\frac{2i(i+1)}{3^{2/5}} (b_{i+1}(i+1)^2 - b_i i^2) \right]^{5/9} \qquad (20)$$

In Figures 5 and 6 the binodal lines (obtained from the precise expressions for the free energy $F^{(i)}$) are plotted as a function of N_A and N_B in the logarithmic coordinates. They indicate good agreement with exponents 10/9 and −16/9 that follow from eq 20. We therefore conclude that the critical ionic strength of the solution (salt concentration c_s) corresponding to abrupt transformations of charged micelles is given by the power law dependence

$$v \simeq \frac{\alpha^2}{c_s} \approx \frac{N_B^{10/9}}{N_A^{16/9}} \qquad (21)$$

5. Discussion and Conclusions

We have developed a mean-field theory which describes micellization of diblock copolymer with one hydrophobic and one polyelectrolyte block in dilute aqueous solution. The theory enables us to predict the ranges of thermodynamic stability and coexistence lines (binodals) for aggregates of different morphologies. We note that our model does not account for the finite size of cylindrical and lamellar micelles and considers only infinitely large aggregates. We also ignored the problem of possible solution instability associated with the cylinder-to-lamella transition. Similarly to neutral block copolymers,[35] the van der Waals attraction between lamellas can cause the aggregation of block copolymer and precipitation of lamellar mesophase in the sediment.

We demonstrated that, similarly to conventional ionic surfactants, the polymeric ionic surfactants can form aggregates of spherical, cylindrical, and lamellar morphologies with progressively increasing salt concentration provided that $N_B \gg N_A$. For $N_A \geq \cong N_B$, the spherical aggregates are thermodynamically optimal at any salt concentration. The transformations between aggregates of different morphologies are the first-order phase transitions that occur upon an increase in salt concentration or/and variation of the pH of the solution (in the case of the pH-sensitive ionic blocks).

The physical mechanism for these transitions is similar to that for low molecular weight surfactants. The dominant terms in the free energy (that determine the structure of aggregates) are the (screened Coulomb) repulsion between the coronal blocks and the excess free energy of the core−water interface. With increasing salt concentration repulsive interactions between the coronal blocks are decreasing. As a result, the optimal surface area per chain decreases and the optimal aggregate size increases. This leads to progressively increasing penalty due to extension of the core blocks.

Transformation of the spherical micelles into cylindrical aggregates (and at higher salt concentration, the transition of cylindrical aggregates into lamellas) leads to relaxation of the core blocks (reduction in their elastic stretching) at almost constant surface area per chain. We emphasize that it is this relaxation of core blocks B that gives rise to the transitions between micelles of different morphologies. Therefore, it is not surprising that these transitions occur in the regime of crew-cut micelles where corona thickness $D - R \ll R$. In the crew-cut spherical and cylindrical micelles, the leading (corresponding to the zero curvature) term in the free energy of micellar corona is the same for all the morphologies, and the difference between the free energies of spheres and cylinders appears only as the first-order correction in curvature. The interplay of these correction terms with the free energy of elastic stretching of the core blocks (that is also a lower order term in comparison to the corona contribution and the excess free energy of the core/corona interface) determines the transition (binodal) line separating different morphologies. The crew-cut structure of micelles at the transition point allowed us to obtain simple analytical (power-law) dependences of the binodals on the parameters of copolymer chain (the lengths of blocks N_A and N_B and the degree of corona ionization α).

The transitions between charged micelles of different morphologies were considered earlier in ref 25. In contrast to our findings, the sphere-to-cylinder and cylinder-to-lamella transitions were localized in ref 25 in the starlike regime of charged aggregates. The origin of this discrepancy is an inadequate extrapolation of the

asymptotic expressions for the free energy of a starlike corona (valid only in the limit of $D \gg R$) to the range of $D \simeq R$. As a result of such treatment, the free energies of the spherical, cylindrical, and lamellar starlike micelles intersected at $D > R$, giving rise to improper location of the sphere-to-cylinder and cylinder-to-lamella transitions. As emphasized earlier, the driving force for morphological transitions is the successive relaxation of elastic stretching of the core blocks in the row sphere−cylinder−lamella. Without this effect, the spherical micelles would be stable at any salt concentration. Indeed, if the full expression for the corona free energy valid at any value of $D/R <$ or > 1 (eq 7) is balanced with the surface free energy, we find $F^{(3)} < F^{(2)} < F^{(1)}$ at any arbitrary value of the effective virial coefficient v. When, however, the elastic stretching of core blocks F_{core} is taken into account, the transition between different morphologies appears in the crew-cut regime.

The general picture of salt-induced evolution of aggregates formed by diblock copolymers with an annealing (weakly dissociating) polyelectrolyte block is more complicated. In our previous study[21] we focused on the spherical micelles with annealing polyelectrolyte corona. The aggregates of different morphologies were not considered. We demonstrated that when pH ≅ pK, the degree of ionization of polyelectrolyte blocks in the chains associated into spherical aggregates and in the individual chains (unimers) in the solution are different. An increase in salt concentration leads not only to the screening of the Coulomb interactions but also to the enhanced ionization of the polyelectrolyte blocks in the corona. The latter effect is analogous to salt-induced ionization of the polyelectrolyte brushes[36] and the coronas or star-branched polyelectrolytes.[37,38] As a result, at relatively low ionic strength in the bulk solution, the salt-induced transitions between different morphologies are expected to have the "inverse" succession. That is, an increase in salt concentration will give rise to the lamella-to-cylinder and the cylinder-to-sphere transitions. These effects will be considered in details in our forthcoming publication.

Acknowledgment. O.V.B. is thankful to R. Netz for a stimulating discussion. O.V.B. acknowledges the hospitality of Professor K. Kremer at the Max-Planck Institute for Polymer Research, Mainz. This work has been partially supported by the Dutch National Science Foundation (NWO) program "Self-Organization and Structure of Bionanocomposits" No. 047.009.016 and by the Russian Foundation for Basic Research (Grant 02-03-33127).

Appendix

Following ref 39, we can present the free energy of a micellar corona (per chain) as

$$F^{(i)}_{corona}/k_BT = \frac{3}{2a^2}\int_R^D \left(\frac{dr}{dn}\right) dr + v\,\frac{s}{R^{i-1}}\int_R^D c_p{}^2(r) r^{i-1} dr \qquad i = 1, 2, 3 \quad \text{(A1)}$$

where the first term accounts for the entropy loses in the nonuniformly extended chain, while the second term account for the osmotic interactions with the effective second virial coefficient v.

Using relation between local chain extension, dr/dn, and the local polymer density, $c_p(r)$

$$c_p(r) = \frac{dn}{s\,dr}\left(\frac{R}{r}\right)^{i-1} \quad \text{(A2)}$$

we can present eq A1 as

$$F^{(i)}_{corona}/k_BT = \int_R^D f\{c_p(r)\}\left(\frac{r}{R}\right)^{i-1} s\,dr \quad \text{(A3)}$$

where $f\{c_p(r)\}$ is the free energy density in the corona. The polymer density profile $c_p(r)$ in a free (nonconfined) corona can be found from the condition of vanishing osmotic pressure

$$\frac{\partial}{\partial c_p(r)}\frac{f\{c_p(r)\}}{c_p(r)} = 0 \quad \text{(A4)}$$

(which can be also obtained from the local force balance condition[40] assuming that the elastic tension at the chain ends is negligible, that is always the case for long chains) that leads to

$$c_p(r) = \left(\frac{3}{vs^2}\right)^{1/3}\left(\frac{R}{r}\right)^{2(i-1)/3} \qquad i = 1, 2, 3 \quad \text{(A5)}$$

Substituting eq A5 into eq A1 and taking into account eq 1, we find

$$F^{(i)}_{corona} = \frac{3^{8/3}}{2(4-i)}\left(\frac{\tau v}{iN_B}\right)^{1/3} R^{4/3}\left[\left(\frac{D}{R}\right)^{(4-i)/3} - 1\right] \quad \text{(A6)}$$

The thickness D of the corona can be determined from the normalization condition

$$\int_R^D c_p(r)\left(\frac{r}{R}\right)^{i-1} s\,dr = N_A \quad \text{(A7)}$$

that leads to the following equation

$$\frac{3^{4/3}}{i+2}\left(\frac{iN_B}{\tau v}\right)^{1/3}\frac{R^{2/3}}{N_A}\left[\left(\frac{D}{R}\right)^{(i+2)/3} - 1\right] = 1$$

to give

$$\frac{D}{R} = \left[1 + \frac{i+2}{3^{4/3}}\left(\frac{\tau v}{iN_B}\right)^{1/3}\frac{N_A}{R^{2/3}}\right]^{3/(i+2)} \quad \text{(A8)}$$

The final expression for the free energy of the corona yields

$$F^{(i)}_{corona} = \frac{3^{8/3}}{2(4-i)}\left(\frac{\tau v}{iN_B}\right)^{1/3} R^{4/3}\left[\left(1 + \frac{i+2}{3^{4/3}}\left(\frac{\tau v}{iN_B}\right)^{1/3}\frac{N_A}{R^{2/3}}\right)^{(4-i)/(i+2)} - 1\right] \quad \text{(A9)}$$

References and Notes

(1) Israelachvili J. N. *Intermolecular and Surface Forces*; Academic Press: London, 1985.
(2) Hunter, R. J. *Foundations of Colloid Science*; Oxford University Press: Oxford, 2002.
(3) Kiserow, D.; Prochazka, K.; Ramireddy, C.; Tuzar, Z.; Munk, P.; Webber, S. E. *Macromolecules* **1992**, *25*, 461.
(4) Khougaz, K.; Astafieva, I.; Eisenberg, A. *Macromolecules* **1995**, *28*, 7135.

(5) Amiel, C.; Sikka, M.; Schneider, J. W.; Tsao, Y. H.; Tirrell, M.; Mays, J. W. *Macromolecules* **1995**, *28*, 3125.
(6) (a) Guenoun, P.; Delsanti, M.; Gaseau, D.; Auvray, L.; Cook, D. C.; Mays, J. W.; Tirrell, M. *Eur. Phys. J. B* **1998**, *1*, 77. (b) Guenoun, P.; Davis, H. T.; Tirrell, M.; Mays, J. W. *Macromolecules* **1996**, *29*, 3965. (c) Guenoun, P.; Muller, F.; Delsanti, M.; Auvray, L.; Chen, Y. J.; Mays, J. W.; Tirrell, M. *Phys. Rev. Lett.* **1998**, *81*, 3872. (d) Muller, F.; Delsanti, M.; Auvray, L.; Yang, J.; Chen, Y. J.; Mays, J. W.; Demé, B.; Tirrell, M.; Guenoun, P. *Eur. Phys. J. E* **2000**, *3*, 45.
(7) Förster, S.; Hemsdorf, N.; Leube, W.; Schnablegger, H.; Regenbrecht, M.; Akari, S.; Lindner, P.; Böttcher, C. *J. Phys. Chem. B* **1999**, *103*, 6657.
(8) (a) Groenewegen, W.; Egelhaalf, S. U.; Lapp, A.; van der Maarel, J. R. C. *Macromolecules* **2000**, *33*, 3283. (b) Groenewegen, W.; Lapp, A.; Egelhaalf, S. U.; van der Maarel, J. R. C. *Macromolecules* **2000**, *33*, 4080.
(9) Schuch, H.; Klingler, J.; Rossmanith, P.; Frechen, T.; Gerst, M.; Feldthusen, J.; Müller, A. H. E. *Macromolecules* **2000**, *33*, 3687.
(10) Förster, S.; Hermsdorf, N.; Böttcher, C.; Lindner, P. *Macromolecules* **2002**, *35*, 4096.
(11) Krämer, E.; Förster, S.; Göltner, C.; Antonietti, M. *Langmuir* **1998**, *14*, 2027. Regenbrecht, M.; Akari, S.; Förster, S.; Möhwald, H. *Surf. Interface Anal.* **1999**, *27*, 418.
(12) Förster, S.; Hermsdorf, N.; Leube, W.; Schnablegger, H.; Regenbrecht, M.; Akari, S.; Lindner, P.; Bttcher, C. *J. Phys. Chem. B* **1999**, *103*, 6652.
(13) Regenbrecht, M.; Akari, S.; Förster, S.; Möhwald, H. *J. Phys. Chem. B* **1999**, *103*, 6668.
(14) Regenbrecht, M.; Akari, S.; Förster, S.; Netz, R. R.; Möhwald, H. *Nanotechnology* **1999**, *10*, 434.
(15) Förster, S.; Abetz, V.; Müller A. H. E. *Adv. Polym. Sci.*, in press.
(16) Marko, J. F.; Rabin, Y. *Macromolecules* **1992**, *25*, 1503.
(17) Wittmer, J.; Joanny, J.-F. *Macromolecules* **1993**, *26*, 2691.
(18) Shusharina, N. P.; Nyrkova, I. A.; Khokhlov, A. R. *Macromolecules* **1996**, *29*, 3167.
(19) Huang, C.; Olivera de la Cruz, M.; Delsanti, M.; Guenoun, P. *Macromolecules* **1997**, *30*, 8019.
(20) Borisov, O. V.; Zhulina, E. B. *Macromolecules* **2002**, *35*, 4472.
(21) Zhulina, E. B.; Borisov, O. V. *Macromolecules* **2002**, *35*, 9191.
(22) (a) Halperin, A. *Macromolecules* **1987**, *20*, 2943. (b) Halperin, A. *Europhys. Lett.* **1989**, *8*, 351. (c) Halperin, A.; Alexander, S. *Macromolecules* **1989**, *22*, 2403.
(23) Birshtein, T. M.; Zhulina, E. B. *Polymer* **1989**, *30*, 170.
(24) Halperin, A. *Polymeric vs Monomeric Amphiphiles: Design Parameters Supramolecular Polymers*; Ciferri, A., Ed.; Marcel Dekker: New York, 2000.
(25) Netz, R. R. *Europhys. Lett.* **1999**, *47*, 391.
(26) For weakly dissociating polyelectrolyte blocks α depends only on pH at sufficiently high salt concentration; that is the case in our analysis. On the contrary, at low salt it does depend also on the aggregation state of the copolymer chain that leads to coupling between ionization and aggregation. We do not consider this case here.
(27) de Gennes, P. G. *Scaling Concepts in Polymer Physics*; Cornell University Press: Ithaca, NY, 1979.
(28) Semenov, A. N. *Sov. Phys. JETP* **1985**, *61*, 733.
(29) Pincus, P. A. *Macromolecules* **1991**, *24*, 2912.
(30) Borisov, O. V.; Birshtein, T. M.; Zhulina, E. B. *J. Phys. II* **1991**, *1*, 521.
(31) Zhulina, E. B.; Borisov, O. V. *Macromolecules* **1996**, *29*, 2618.
(32) (a) Watanabe, H.; Patel, S. S.; Argillier, J. F.; Parsonage, E. E.; Mays, J.; Dan-Brandon, N.; Tirrell, M. *Mater. Res. Soc. Symp. Proc.* **1992**, *249*, 255. (b) Mir, Y.; Auroy, P.; Auvray, L. *Phys. Rev. Lett.* **1995**, *75*, 2863. (c) Guenoun, P.; Schlachli, A.; Sentenac, D.; Mays, J. W.; Benattar, J. J. *Phys. Rev. Lett.* **1995**, *74*, 3628. (d) Ahrens, H.; Förster, S.; Helm, C. A. *Phys. Rev. Lett.* **1999**, 4798.
(33) Guo, X.; Ballauff, M. *Phys. Rev. E* **2001**, *64*, 05146.
(34) The condition of salt dominance in the brush implies that concentration of added salt inside (and outside) the brush exceeds the concentration of counterions trapped inside the brush and neutralizing the bare charge of the polyelectrolyte chains.
(35) Zhulina, E. B.; Rubinstein, M. Manuscript in preparation.
(36) Zhulina E. B.; Birshtein, T. M.; Borisov, O. V. *Macromolecules* **1995**, *28*, 1491.
(37) Borisov, O. V.; Zhulina, E. B. *Eur. Phys. J. B* **1998**, *4*, 205.
(38) Klein Wolterink, J.; van Male, J.; Cohen Stuart, M.; Koopal, L. K.; Zhulina, E. B.; Borisov, O. V. *Macromolecules* **2002**, *35*, 9176.
(39) Zhulina, E. B.; Borisov, O. V.; Pryamitsyn, V. A.; Birshtein, T. M. *Macromolecules* **1991**, *24*, 140.
(40) If $t(r) = 3\ dr/dn$ is local elastic tension in the chain, then the force balance for the segment of the chain localized between r and $r + \Delta r$ assumes the form $t(r) - t(r + \Delta r) = \pi(r)s(r) - \pi(r + \Delta r)s(r + \Delta r)$, where $\pi(r)$ and $s(r) = s(r/R)^{i-1}$ are the excess osmotic pressure and the area per chain at coordinate r. Assuming $\pi(D) = 0$ and integrating from r to D, we obtain $t(r) = \pi(r)s(r) - t(D)$. For sufficiently long chains one can safely set $t(D) = 0$, i.e., assume vanishing tension at the chain ends. Then eq A4 is recovered.

MA0304628